nature geoscience

Article

https://doi.org/10.1038/s41561-024-01556-5

Centennial-scale variations in the carbon cycle enhanced by high obliquity

Received: 27 May 2024

Accepted: 11 September 2024

Published online: 11 October 2024

Check for updates

Etienne Legrain[1,2,3] ✉, Emilie Capron[1], Laurie Menviel[4,5], Axel Wohleber[1], Frédéric Parrenin[1], Grégory Teste[1], Amaëlle Landais[6], Marie Bouchet[6], Roberto Grilli[1], Christoph Nehrbass-Ahles[7,8], Lucas Silva[9], Hubertus Fischer[9] & Thomas F. Stocker[9]

Centennial-scale increases of atmospheric carbon dioxide, known as carbon dioxide jumps, are identified during deglacial, glacial and interglacial periods and linked to the Northern Hemisphere abrupt climate variations. However, the limited number of identified carbon dioxide jumps prevents investigating the role of orbital background conditions on the different components of the global carbon cycle that may lead to such rapid atmospheric carbon dioxide releases. Here we present a high-resolution carbon dioxide record measured on an Antarctic ice core between 260,000 and 190,000 years ago, which reveals seven additional carbon dioxide Jumps. Eighteen of the 22 jumps identified over the past 500,000 years occurred under a context of high obliquity. Simulations performed with an Earth system model of intermediate complexity point towards both the Southern Ocean and the continental biosphere as the two main carbon sources during carbon dioxide jumps connected to Heinrich ice rafting events. Notably, the continental biosphere appears as the obliquity-dependent carbon dioxide source for these abrupt events. We demonstrate that the orbital-scale external forcing directly impacts past abrupt atmospheric carbon dioxide changes.

Understanding the mechanisms of natural centennial-scale changes in the carbon cycle is a major challenge under the ongoing anthropogenic carbon dioxide (CO_2)-driven climate change. Recent efforts to produce high-resolution atmospheric CO_2 records from Antarctic ice cores demonstrated the pervasive character of centennial-scale atmospheric CO_2 increases (carbon dioxide jumps, CDJs) in the global climate system over the last 500 ka (thousand years before present)[1]. These CDJs consist of an atmospheric CO_2 increase from ~5 ppm up to ~16 ppm that occurs in a few decades to centuries at estimated rates of up to 26 ppm per century in the atmosphere[1]. The CDJs are identified through thresholds applied on detrended ice-core CO_2 records (amplitude larger than 5 ppm and growth rate equal or above 1.5 ppm per century after removing the orbital trend)[1]. Hence, they only represent the strongest centennial-scale atmospheric CO_2 increases. Two types of Northern Hemisphere climatic event are associated with the CDJs: (1) the Dansgaard–Oeschger (DO) events, which are identified during the last glacial period in Greenland[2,3] and North Atlantic[4] archives. Each DO event is characterized by an abrupt transition from cold, *stadial*,

[1]Université Grenoble Alpes, CNRS, INRAE, IRD, Grenoble INP, IGE, Grenoble, France. [2]Laboratoire de Glaciologie, Université libre de Bruxelles, Brussels, Belgium. [3]Department of Water and Climate, Vrije Universiteit Brussel, Brussels, Belgium. [4]Climate Change Research Centre, University of New South Wales, Sydney, New South Wales, Australia. [5]The Australian Centre for Excellence in Antarctic Science, University of New South Wales, Sydney, New South Wales, Australia. [6]Laboratoire des Sciences du Climat et de l'Environnement, LSCE/IPSL, CEA-CNRS-UVSQ, Université Paris-Saclay, Gif-sur-Yvette, France. [7]Department of Earth Sciences, University of Cambridge, Cambridge, UK. [8]National Physical Laboratory, Teddington, UK. [9]Climate and Environmental Physics, Physics Institute, Oeschger Centre for Climate Change Research, University of Bern, Bern, Switzerland. ✉e-mail: etienne.legrain@ulb.be

to milder, *interstadial*, conditions associated with a Greenland surface temperature increase of 5 to 16 °C in less than a century[5]. We stress that a CDJ with a minimum amplitude of 5 ppm cannot be detected for all DO warmings; (2) the maximum intensity of Heinrich events (HE) within the Heinrich stadials (HS), that is, cold stadial periods in glacial times during which Heinrich iceberg discharge events occurred, as reflected in peaks of ice rafted debris (IRD) in North Atlantic sediment cores[6]. The CDJs occurring at the onset of a DO event (hereafter CDJ+)[1] are associated with an increase in atmospheric methane (CH_4) concentrations larger than 50 ppb (ref. 7). The CDJs occurring within a HS (hereafter CDJ−)[1] are associated with a short and smaller CH_4 increase[1] happening within the HS and probably when maximum iceberg discharge led to further reduction of the AMOC (Atlantic Meridional Overturning Circulation). Proposed hypotheses to explain how these rapid atmospheric CO_2 increases relate to DO events or HE involve both terrestrial[8,9] and marine CO_2 sources[10,11], but overall, the underlying mechanisms remain poorly understood.

Here we argue that the orbital-scale climatic background conditions modulate the intensity of the centennial-scale carbon cycle response to the Northern Hemisphere climatic perturbations. To test this hypothesis, we extend the time interval covered by high-resolution atmospheric CO_2 reconstructions to allow the identification of additional potential CDJs under varying orbital configurations. Then we investigate the impact of orbital-scale changes in the climatic background on centennial-scale CO_2 increases through simulations performed with an Earth system model of intermediate complexity.

Sub-millennial-scale atmospheric CO_2 record

We measured the CO_2 concentrations on the air trapped in 203 samples from the Antarctic EPICA Dome C (EDC) ice core between 260 and 190 ka using a dry-extraction system coupled to a gas chromatograph[12] (Methods). Our CO_2 record is in agreement with published data[13] whereas the mean temporal resolution is higher, 340 years on average (Fig. 1 and Supplementary Fig. 1). We identify seven new CDJs using the detection methodology described in ref. 1. In summary, we first remove the orbital-scale (that is, deglaciation and glaciation) and millennial-scale (that is, Antarctic Isotope Maximum events) imprint in the CO_2 record using cubic smoothing splines[14]. Second, we calculate the rate of change of the detrended CO_2 record and third, we apply thresholds of 1.5 ppm per century for the minimum rate of increase and 5 ppm for the minimum amplitude from ref. 1 to identify CDJs (Methods and Supplementary Figs. 2 and 3). In our record, we identify two CDJs+ associated with atmospheric CH_4 increases higher than 50 ppb in less than 300 years (CDJ+7e and CDJ+7a), three CDJs− that are not associated with a detectable increase in atmospheric CH_4 in the ice-core record and that can be linked to an IRD peak in the oceanic record (CDJ−8a.1, CDJ−8a.2, CDJ−8a.3) and two CDJs that are not associated with either of these two markers (CDJ 7c, CDJ 7b) (Fig. 1 and Supplementary Figs. 3 and 4). Two CDJs occurred during interglacial conditions[15] (CDJ 7b, CDJ+7a) when Northern Hemisphere ice sheets had shrunk to a size approaching the Holocene value, confirming the occurrence of CDJs during periods of relatively small global ice-sheet volume[1] (Fig. 1 and Supplementary Fig. 5). Hence, combining published and newly described events, we highlight 22 CDJs occurring under a wide range of climatic and orbital boundary conditions over the past 500 ka (Fig. 2, Supplementary Fig. 6 and Supplementary Table 1).

Carbon cycle variability and obliquity state

The sources and mechanisms behind centennial-scale releases of atmospheric CO_2 have been investigated previously based on carbon isotope measurements on Antarctic ice and carbon cycle modelling[8,16]. Two main hypotheses have been discussed: (1) the role of a terrestrial carbon source due to a southward shift in the intertropical convergence zone[8,17] and (2) an increase of upwelling activity in the Southern Ocean and/or the North Pacific Ocean possibly due to enhanced intensity or location relative to the sea-ice edge of winds[10,18]. However, the role played by long-term forcing on the centennial-scale CO_2 variability has not yet been assessed.

Here we investigate the potential role of the long-term forcing, for example, the global ice volume and the orbital forcing, on the occurrence of CDJs. We show that 18 of the 22 CDJs occurred at times above the average obliquity value (23.33°) of the 12 obliquity cycles of the last 500 ka (Fig. 2 and Supplementary Fig. 5). We note that seven of the eight obliquity maxima between 416 and 9 ka covered by high-resolution CO_2 and CH_4 data that allow the identification of CDJ occurrences show at least one CDJ. Reversely, only two out of the seven obliquity minima covered by high-resolution CO_2 data are linked to a CDJ (Fig. 2). We investigate the hypothesis of a coincidental origin of this specific pattern of CDJs relative to obliquity changes performing a statistical chi-square test (Methods). According to our analysis, the null hypothesis that centennial-scale release of CO_2 is independent of the obliquity state can be rejected with 90% confidence ($p < 0.1$). Reversely, the occurrence of CDJs is not significantly coupled to the changes in climatic precession, eccentricity and global ice volume (Supplementary Fig. 5 and Supplementary Table 2). Note that our results are independent from the ice-core gas chronology used to display the CO_2 record[19–22] and the choice of orbital solutions[23,24] (Supplementary Fig. 7 and Supplementary Table 3). In addition, whereas our results are obtained using the threshold detection values from ref. 1, sensitivity tests show that obliquity dependence of the CDJ occurrences is robust regardless of the specific threshold values considered (Supplementary Fig. 8 and Supplementary Table 4). Finally, the AMOC variability itself, at the origin of the CDJs, seems not directly related to obliquity. Indeed, most of AMOC variability occurs under a CO_2 concentration window of 190–225 ppm (ref. 25), which corresponds to periods equally distributed between high (50.7%) and low (49.3%) obliquity over the past 500 ka.

Modelling assessment of CO_2 sources during CDJs− events

CDJs− are most likely associated with a complete AMOC shutdown that occurs sometime within the HS[1]. To study the impact of such an AMOC shutdown on the centennial-scale atmospheric CO_2 response, we perform a suite of sensitivity experiments to mimic the carbon cycle response to a HS under both high- and low-obliquity boundary conditions with the Earth System Model LOVECLIM[26]. We propose that HS 5 is the most appropriate HS to use as a case study because the corresponding CDJ occurs during a period characterized by the highest obliquity value (24.3°).

We perform four simulations under 49 ka boundary conditions, that is, with realistic orbital parameters, including an obliquity value of 24.3° and an estimate of Northern Hemispheric ice-sheet extent, topography and associated albedo[26] (Methods and Supplementary Table 5). We also perform four simulations under the same boundary conditions except for an obliquity value of 22.1°, that is, the lowest value of the last 500 ka (Supplementary Table 5). In all experiments, an idealized HE is simulated by adding 0.3 Sverdrup (Sv) of freshwater to the North Atlantic (60–10° W, 50–60° N) during 1,000 years, to induce an AMOC shutdown (Supplementary Fig. 9). The sequence of changes during HS is still debated and especially the role of freshwater flux in the observed AMOC weakening[7,27]. Nevertheless, previous modelling studies have shown that the simulated climatic response to an AMOC weakening was similar whether the freshwater flux had an active (hosed) or passive (unhosed) role[28].

The simulation conducted under 49 ka climatic conditions (*HighObl*) reveals a centennial-scale response of the carbon cycle to the induced freshwater perturbation (Fig. 3a), characterized by an ~9.5 ppm increase in atmospheric CO_2 over the first 400 years of the simulation (Fig. 3a,c, Supplementary Table 5 and Supplementary Fig. 10). A similar simulation performed under low obliquity (*LowObl*) only leads to an ~3.3 ppm CO_2 increase over the first 400 years following

https://doi.org/10.1038/s41561-024-01556-5

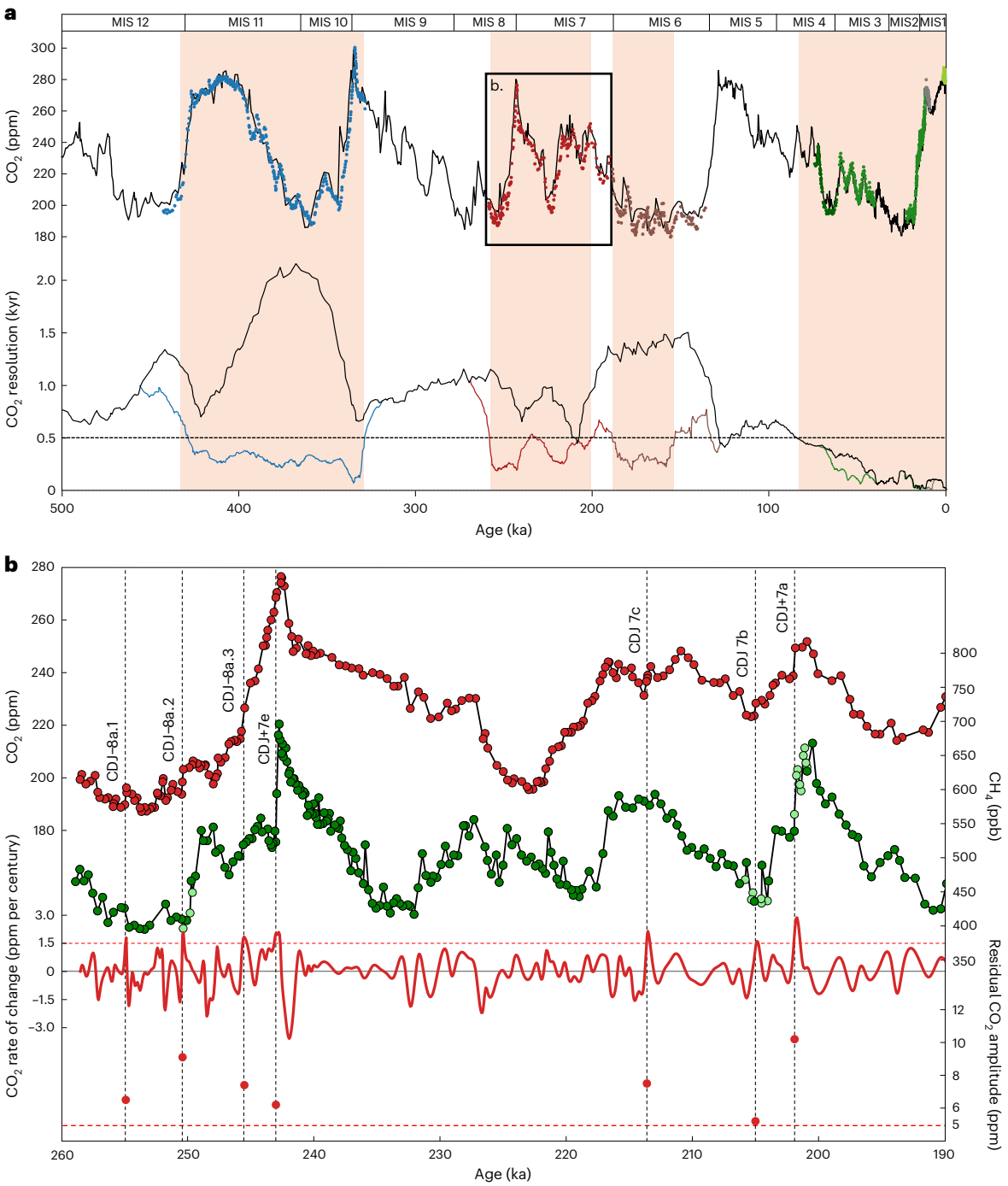

Fig. 1 | Improvement of the temporal resolution of the ice-core atmospheric CO_2 record since the composite CO_2 record from ref. 44 over the last 500 ka. **a**, At the top, high-resolution records are represented in blue[1], red (this study), brown[12], green[8], dark green[45], grey[46] and light-green dots[47], plotted on their own published age scales. They are superimposed on the composite CO_2 record[44] (black line). At the bottom, temporal resolutions of all records computed as the running mean of 20 data points (colour codes similar to top panel). Data are not corrected for potential offsets due to the use of different experimental set-ups. Shaded red bands indicate periods where the ice-core CO_2 record is associated with a temporal resolution better than 500 years. **b**, At the top, zoom on our EDC CO_2 record between 260 and 190 ka (red dots, black line) and CH_4 record from this study (light green) and previous studies[48,49] (dark green) plotted on the Antarctic Ice Core Chronology 2023 (AICC2023) timescale[22]. Vertical black dashed lines indicate the newly identified CDJs (Methods). In the middle, CO_2 rates of change from the detrended CO_2 record for the smoothing spline (1 kyr cut-off period)[1]. At the bottom, residual CO_2 amplitude of the detrended CO_2 record during the events occurring at a rate higher than 1.5 ppm per century. Vertical back dashed lines indicate the timing of the identified CDJs. A centennial-scale CO_2 release is identified when the rate is higher than 1.5 ppm per century and the amplitude is higher than 5 ppm (dashed horizontal red lines)[1]. MIS: Marine Isotope Stage.

the freshwater perturbation (Fig. 3c and Supplementary Table 5). In both experiments, the CO_2 increase is due to a terrestrial carbon release due to climatic changes induced by the AMOC weakening (Fig. 3d and Supplementary Fig. 9). Surface air temperature is lower under low obliquity, particularly in the Northern Hemisphere (−1.4 °C north of 20° N), thus impacting the precipitation patterns (Fig. 4a). As a result, the terrestrial carbon reservoir is smaller under low than high obliquity (−105 gigatons of carbon, GtC; Fig. 4b). The decrease of precipitation

https://doi.org/10.1038/s41561-024-01556-5

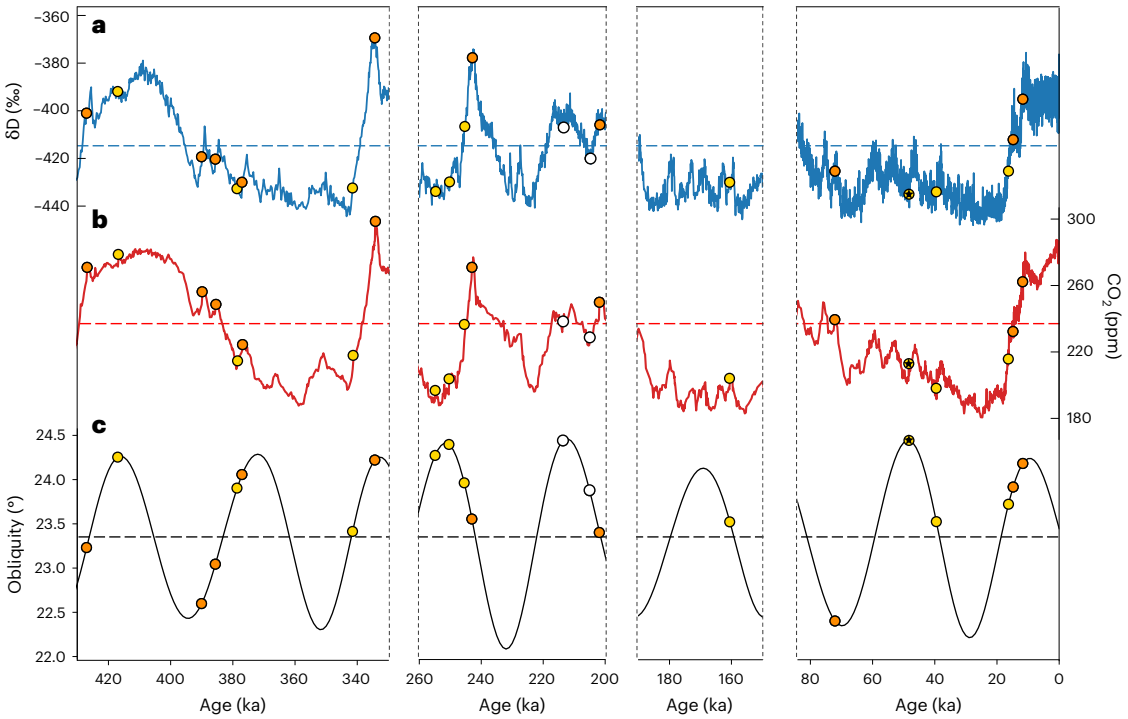

Fig. 2 | Climatic and obliquity states for centennial-scale releases of atmospheric CO_2 during the three periods associated with high-resolution ice-core CO_2 records. a, EDC deuterium record (δD)[50] on the AICC2023 ice age scale[22] (blue line). **b**, Atmospheric CO_2 high-resolution records on the AICC2023 gas age scale[22] for the time interval 500–67 ka, on the WD2014[51,52] timescale for the 67–12-ka interval and on several original timescales for the 12–0 ka interval (this study; refs. 1,8,12,44–47; red line). **c**, Obliquity[24] (black). Horizontal dashed lines indicate the average value for each considered proxy record over the last 500 ka. Yellow, orange and white dots indicate the value of the record during the occurrence of CDJ−, CDJ+ and undetermined CDJ, respectively[1,8,17]. The CDJ− identified during HS 5 (~49 ka) and simulated with LOVECLIM is identified with black stars on the three represented climate variables.

and the lower temperature over the northern high latitudes during the freshwater input thus leads to a smaller terrestrial carbon release under low obliquity compared with high obliquity.

To investigate the role of terrestrial carbon release, two freshwater experiments are performed in which carbon fluxes between the continental biosphere and the atmosphere are suppressed. Under such conditions, neither the experiment performed under high obliquity (*HighObl_noVeg*) nor the one performed under low obliquity (*LowObl_NoVeg)* produce a centennial-scale CO_2 event (that is, ~0 ppm CO_2 change at year 400; Fig. 3c, Supplementary Fig. 11 and Supplementary Table 5). Those results highlight that the obliquity no longer has an influence on the centennial-scale CO_2 variability if the continental biosphere is muted. They point to the continental biosphere as the variable source of carbon at centennial scale for CDJ− events, which appears strongly controlled by Earth's obliquity.

Additional experiments were conducted to investigate the impact of obliquity on the CDJ+ occurring at the end of the Younger Dryas (YD) (~12 ka) (ref. 17) (Methods). Our LOVECLIM simulations forced with constant 12-ka boundary conditions are not able to reproduce the magnitude and duration of the CDJ+ event, regardless of the obliquity forcing applied (Supplementary Figs. 21 and 22). A decrease in CO_2 solubility due to ocean warming[29] or strengthening/poleward shift of the Southern Hemisphere Westerlies (SHW), as suggested for the end of the YD[10,30], might be necessary to simulate such a rapid CO_2 increase[31].

A stronger CO_2 release from the Southern Ocean, potentially resulting from enhanced Southern Ocean upwelling has been suggested as a process leading to CDJ− during Termination I[10]. Enhanced upwelling of CO_2-rich waters in the Southern Ocean could result from a poleward shift of the sea-ice edge[10] or intensified (and/or poleward shifted) SHW during HS[31]. The robustness of the modelled responses to such wind changes was tested by conducting two additional simulations with an imposed ~40% increase of the SHW wind stress, one under 49-ka conditions (*HighObl_SHW*) and one under low-obliquity conditions (*LowObl_SHW)* (Supplementary Table 5). This leads to a stronger CO_2 release during both high- and low-obliquity conditions. However, the difference in total CO_2 release between high- and low-obliquity conditions persists and only exists when the terrestrial biosphere exchanges CO_2 with the atmosphere. These results reinforce the idea that the SHW play a role in centennial-scale carbon cycle increases (Fig. 3a and Supplementary Table 5). However, larger CO_2 changes are simulated when terrestrial vegetation and enhanced SHW (*HighObl*_SHW and *LowObl_SHW*) are considered. Our results show that the terrestrial biosphere reservoir is the main source of the higher carbon release during high-obliquity conditions for CDJ− events due to its apparent sensitivity to the obliquity context.

Now we compare the magnitude and duration of the centennial-scale atmospheric CO_2 variations recorded in the West Antarctic Ice Sheet (WAIS) Divide ice core (WDC) across HS 5 (~49 ka) and those modelled in the simulations that include terrestrial carbon fluxes. We look at the CO_2 difference between the high- and low-obliquity simulations (ΔCO_2; Fig. 3b). The ΔCO_2 value allows to identify the difference of amplitude of the modelled centennial-scale response of atmospheric CO_2 concentrations in the high-obliquity vs low-obliquity simulations. ΔCO_2 increases at centennial scale and reaches a maximum around year 400 (Fig. 3b and Supplementary Fig. 10). In terms of magnitude, this ΔCO_2 partially explains the recorded centennial-scale variability in the WDC CO_2 record. This comparison illustrates a similar temporal structure between the measured and simulated CO_2 changes. After year 1,000, the WDC CO_2 changes are decoupled from the variations of the simulated ΔCO_2, revealing a change in the dynamics of the carbon cycle from centennial scale to millennial scale most likely not related to obliquity state. Whereas this model–data comparison is limited by

https://doi.org/10.1038/s41561-024-01556-5

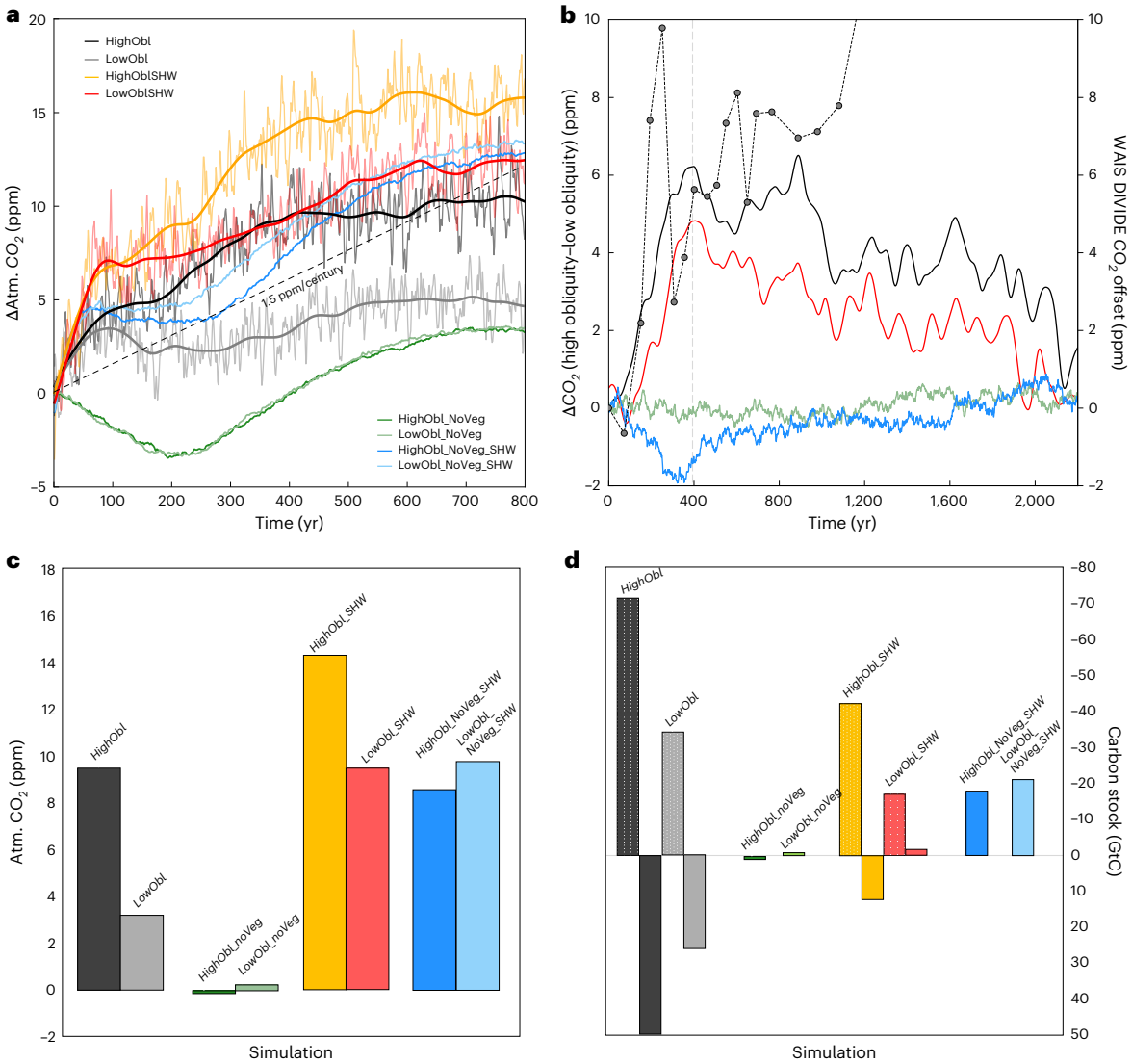

Fig. 3 | Simulated carbon cycle response to an AMOC shutdown. a, Evolution of atmospheric CO_2 for the eight simulations as a function of time. The dashed grey line corresponds to a 1.5 ppm per century CO_2 increase, which is also the threshold used to identify CDJ events in the ice-core CO_2 record. Bold lines are smoothing spline filters. **b**, ΔCO_2 between *HighObl–LowObl* (black line), *HighObl_SHW–LowObl_SHW* (red line), *HighObl_NoVeg–LowObl_NoVeg* (green line) and *HighObl_NoVeg_SHW–LowObl_NoVeg_SHW* (blue line). SHW, Southern Hemisphere Westerlies; Veg, vegetation. A positive value means that the CO_2 anomaly due to the perturbation is higher under a high-obliquity phase than under a low-obliquity phase. Grey dots with dashed line correspond to the atmospheric CO_2 record from the West Antarctic Ice Sheet (WAIS) ice core during HS 5, the HS that is simulated in the present study. **c**, Paired coloured bars correspond to the atmospheric CO_2 offset values 400 years after the freshwater perturbation for simulations using the obliquity value at 49 ka (left, 24.3°) and a prescribed low-obliquity value (right, 22.1°). Words in italic refer to simulation names. **d**, Same simulation results as in **c** but with carbon stock in GtC. Negative carbon anomaly represents a carbon release from that reservoir into the atmosphere. Plain coloured bars represent the oceanic carbon stock, and coloured bars with white dots represent the terrestrial carbon stock. Colours refer to the same simulation as in **c**. The year 400 snapshot represents the period with the largest atmospheric CO_2 difference between the high- and low-obliquity simulations and corresponds to a time period where most of the CO_2 response to the freshwater forcing has occurred (Supplementary Fig. 10).

the modelling design, it supports our hypothesis that the orbital-scale obliquity changes influence centennial-scale carbon cycle variations through the terrestrial carbon reservoir.

Drivers of centennial-scale atmospheric CO_2 increases

Previous studies have evidenced an acidification of the Southern Ocean[10,11] and of the North Pacific Ocean[18] synchronous with the CDJ+ occurring at the onsets of the Bolling Allerød and of the Holocene. This would be consistent with an enhanced CO_2 outgassing in the Southern Ocean resulting from the interplay between the location of the SHW and the sea-ice edge that could have also contributed to previous CDJ+ events[10]. Our modelling results show that variations in SHW can act as a key driver of a centennial-scale carbon cycle. However, the SHW changes resulting from an AMOC shutdown could also be modulated by obliquity. Hence, we cannot exclude the hypothesis that the Southern Ocean is an obliquity-dependent source of CO_2, and additional simulations investigating the link between SHW and obliquity should be performed with alternative models.

Our simulations indicate that the continental biosphere provides an additional source of carbon to the atmosphere during CDJ− events, as already inferred by modelling or carbon isotope approaches[8,32,33] and reveals the obliquity dependence of this carbon source at centennial scale. Especially the region between 8° N and 40° N appears as the

https://doi.org/10.1038/s41561-024-01556-5

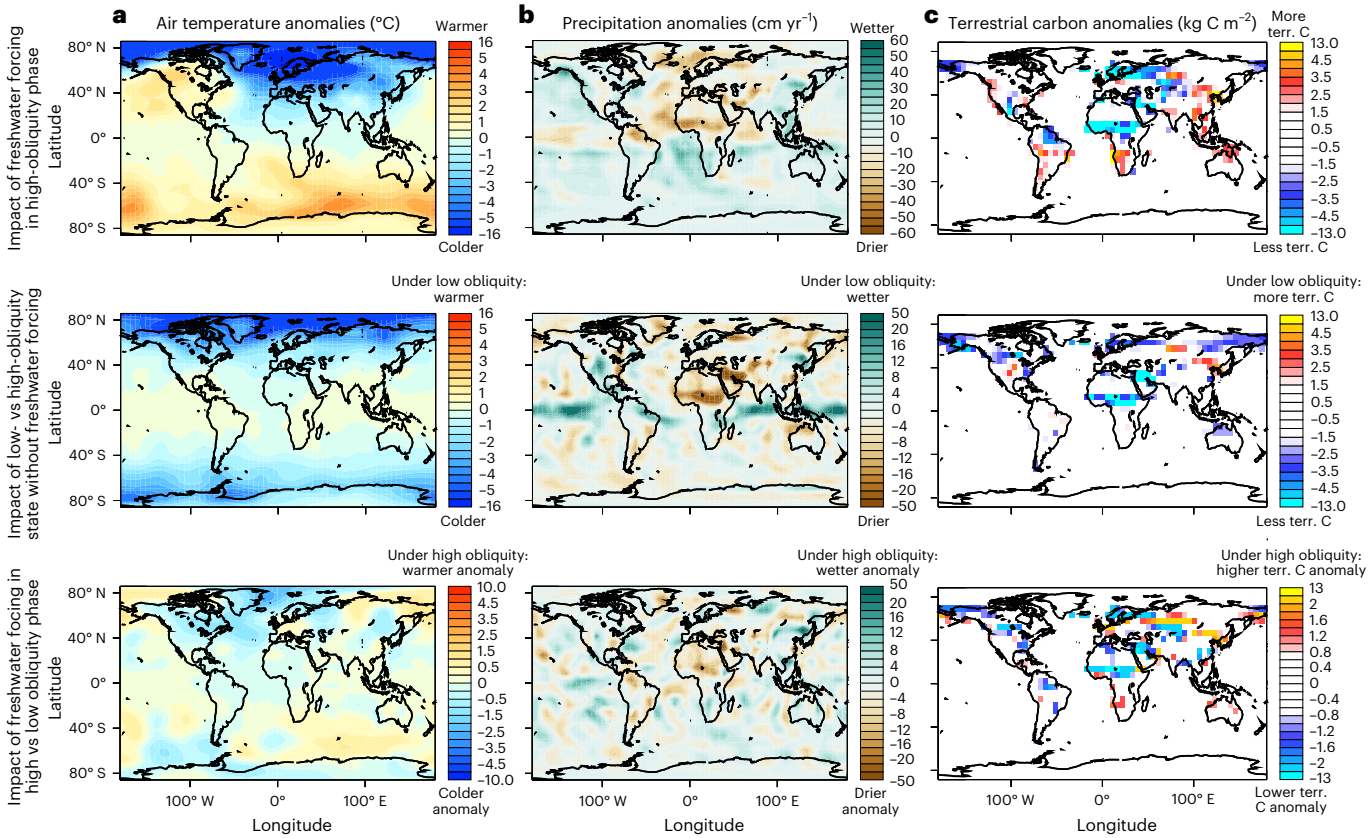

Fig. 4 | Simulated impacts of the freshwater forcing and the obliquity state on the climatic conditions and terrestrial carbon stock. a, Air temperature anomalies resulting from (top) a freshwater forcing under a high-obliquity phase vs no freshwater forcing under a high-obliquity phase (*HighObl–HighOblCTR*), (middle) a low-obliquity phase without a freshwater forcing vs a high-obliquity phase without a freshwater forcing *(LowOblCTR–HighOblCTR)* and (bottom) the impact of the freshwater forcing in a high- vs low-obliquity phase *(HighObl–HighOblCTR)–(LowObl–LowOblCTR)* on air temperatures. **b**, Same as **a** for precipitation anomalies. **c**, Same as **a** for the terrestrial carbon anomalies. Basemap outlines from ETOPO5 Global relief model (https://www.ncei.noaa.gov/products/etopo-global-relief-model). CTR, control; terr., terrestrial. Figure/panel created with Ferret.

additional source of terrestrial carbon under a high-obliquity phase (Fig. 4c). Previous studies revealed an orbital- and millennial-scale control of obliquity on vegetation changes based on pollen[34,35] and sediment records[36,37] and through modelling approaches[38]. This obliquity control modulates the carbon stock available to be released during centennial-scale increases through the extent and type of vegetation. In the low-latitude regions, the induced southward shift of the Inter Tropical Convergence Zone and changes in latitudinal insolation gradients[38] cause an obliquity-paced vegetation change especially for subtropical biomes and tree coverage[34,37]. Depending on the area considered in the mid-latitudes regions, both precession and obliquity forcing seem to be the main drivers of the Asian monsoon system and hence of the induced summer precipitation that controls the vegetation coverage in the area[36]. At higher latitudes, the predominance of trees and shrubs over grasses and herbs is favoured under high obliquity due to lower local ice extent[35]. Our study suggests that the expansion of continental biomass in the high latitudes and the change of vegetation at low latitudes in high-obliquity phases could thus provide a large amount of carbon to be released during CDJ– (Fig. 3d). In principle, this additional carbon is also available for enhanced terrestrial carbon release during CDJ+ under high-obliquity conditions. With respect to the opposite latitudinal shift of the Inter Tropical Convergence Zone between DO and HE, a similar obliquity dependence on the terrestrial biosphere carbon release is also possible. However, our model experiments performed at 12 ka did not successfully reproduce the magnitude and duration of the CDJ+. Additional model experiments would need to be performed to corroborate the influence of obliquity on CDJ+ events.

To conclude, our study confirms a joint contribution of terrestrial and oceanic carbon release during CDJ– events and points towards the terrestrial carbon reservoir as a variable sensitive to obliquity in this centennial-scale response.

Under the conditions of the glacial–interglacial cycles during the last 600 ka, a strong imprint of both obliquity[34,35,37,38] and precession[39,40] was demonstrated for regional variability of vegetation and climate. Our CDJs compilation reveals no direct correlation between precession and CDJ occurrences over the past 500 ka (Supplementary Fig. 5), and our simulations confirm the quantitative impact of obliquity on centennial-scale variability of terrestrial carbon fluxes during CDJ– (Fig. 4). Still, future simulations investigating if changes in precession influence centennial-scale atmospheric CO_2 release would be useful.

Our results reinforce the importance of producing carbon isotope and oceanic pH records during CDJ periods to confirm the processes leading to centennial-scale atmospheric CO_2 increases. In addition, further modelling studies of both CDJ+ and CDJ– events should be conducted to confirm the pervasive character of the identified mechanism. Here we show that past centennial-scale atmospheric CO_2 increases with associated AMOC disruption were more likely to happen during high-obliquity phases. Five of the past CDJs occurred under an obliquity value that is close to the current one (±5% of the range of the obliquity value variability of the last 500 ka). Whereas a 15% weakening of the AMOC since the mid-twentieth century has been estimated[41], large uncertainties remain on the potential occurrence of a large AMOC disruption at multi-centennial scale in the future[42,43]. If such AMOC disruption occurs, the current relatively high-obliquity

phase is favourable to a measurable release of carbon into the atmosphere, which would superimpose onto the anthropogenic-sourced perturbation. This release, which could last from a few decades to a few centuries, would be equivalent to ~4 years of CO_2 anthropogenic emissions at the 2010–2019 emissions rate.

Online content

Any methods, additional references, Nature Portfolio reporting summaries, source data, extended data, supplementary information, acknowledgements, peer review information; details of author contributions and competing interests; and statements of data and code availability are available at https://doi.org/10.1038/s41561-024-01556-5.

References

1. Nehrbass-Ahles, C. et al. Abrupt CO_2 release to the atmosphere under glacial and early interglacial climate conditions. *Science* **369**, 1000–1005 (2020).
2. Capron, E. et al. The anatomy of past abrupt warmings recorded in Greenland ice. *Nat. Commun.* **12**, 2106 (2021).
3. North Greenland Ice Core Project members. High-resolution record of Northern Hemisphere climate extending into the last interglacial period. *Nature* **431**, 147–151 (2004).
4. Voelker, A. H. L. Global distribution of centennial-scale records for Marine Isotope Stage (MIS) 3: a database. *Quat. Sci. Rev.* **21**, 1185–1212 (2002).
5. Kindler, P. et al. Temperature reconstruction from 10 to 120 kyr b2k from the NGRIP ice core. *Clim* **10**, 887–902 (2014).
6. Ruddiman, W. F. Late Quaternary deposition of ice-rafted sand in the subpolar North Atlantic (lat 40° to 65°N). *Geol. Soc. Am. Bull.* **88**, 1813 (1977).
7. Rhodes, R. H. et al. Enhanced tropical methane production in response to iceberg discharge in the North Atlantic. *Science* **348**, 1016–1019 (2015).
8. Bauska, T. K., Marcott, S. A. & Brook, E. J. Abrupt changes in the global carbon cycle during the last glacial period. *Nat. Geosci.* **14**, 91–96 (2021).
9. Bauska, T. K. et al. Carbon isotopes characterize rapid changes in atmospheric carbon dioxide during the last deglaciation. *Proc. Natl Acad. Sci. USA* **113**, 3465–3470 (2016).
10. Rae, J. W. B. et al. CO_2 storage and release in the deep Southern Ocean on millennial to centennial timescales. *Nature* **562**, 569–573 (2018).
11. Ronge, T. A. et al. Southern Ocean contribution to both steps in deglacial atmospheric CO_2 rise. *Sci. Rep.* **11**, 22117 (2021).
12. Shin, J. et al. Millennial-scale atmospheric CO_2 variations during the Marine Isotope Stage 6 period (190–135 ka). *Clim* **16**, 2203–2219 (2020).
13. Petit, J. R. et al. Climate and atmospheric history of the past 420,000 years from the Vostok ice core. *Nature* **399**, 429–436 (1999).
14. Enting, I. G. On the use of smoothing splines to filter CO_2 data. *J. Geophys. Res.* **92**, 10977 (1987).
15. Past Interglacials Working Group of PAGES. Interglacials of the last 800,000 years. *Rev. Geophys.* **54**, 162–219 (2016).
16. Bauska, T. K. et al. Controls on millennial-scale atmospheric CO_2 variability during the last glacial period. *Geophys. Res. Lett.* **45**, 7731–7740 (2018).
17. Marcott, S. A. et al. Centennial-scale changes in the global carbon cycle during the last deglaciation. *Nature* **514**, 616–619 (2014).
18. Gray, W. R. et al. Deglacial upwelling, productivity and CO_2 outgassing in the North Pacific Ocean. *Nat. Geosci.* **11**, 340–344 (2018).
19. Bazin, L. et al. An optimized multi-proxy, multi-site Antarctic ice and gas orbital chronology (AICC2012): 120–800 ka. *Clim* **9**, 1715–1731 (2013).
20. Veres, D. et al. The Antarctic ice core chronology (AICC2012): an optimized multi-parameter and multi-site dating approach for the last 120 thousand years. *Clim* **9**, 1733–1748 (2013).
21. Extier, T. et al. On the use of $\delta^{18}O_{atm}$ for ice core dating. *Quat. Sci. Rev.* **185**, 244–257 (2018).
22. Bouchet, M. et al. The Antarctic Ice Core Chronology 2023 (AICC2023) chronological framework and associated timescale for the European Project for Ice Coring in Antarctica (EPICA) Dome C ice core. *Clim* **19**, 2257–2286 (2023).
23. Berger, A. & Loutre, M. F. Insolation values for the climate of the last 10 million years. *Quat. Sci. Rev.* **10**, 297–317 (1991).
24. Laskar, J. et al. A long-term numerical solution for the insolation quantities of the Earth. *AA* **428**, 261–285 (2004).
25. Vettoretti, G., Ditlevsen, P., Jochum, M. & Rasmussen, S. O. Atmospheric CO_2 control of spontaneous millennial-scale ice age climate oscillations. *Nat. Geosci.* **15**, 300–306 (2022).
26. Goosse, H. et al. Description of the Earth system model of intermediate complexity LOVECLIM version 1.2. *Geosci. Model Dev.* **3**, 603–633 (2010).
27. Barker, S. et al. Icebergs not the trigger for North Atlantic cold events. *Nature* **520**, 333–336 (2015).
28. Brown, N. & Galbraith, E. D. Hosed vs. unhosed: interruptions of the Atlantic Meridional Overturning Circulation in a global coupled model, with and without freshwater forcing. *Clim* **12**, 1663–1679 (2016).
29. Menviel, L., England, M. H., Meissner, K. J., Mouchet, A. & Yu, J. Atlantic-Pacific seesaw and its role in outgassing CO_2 during Heinrich events: Heinrich CO_2. *Paleoceanography* **29**, 58–70 (2014).
30. Gray, W. R. et al. Poleward shift in the southern hemisphere westerly winds synchronous with the deglacial rise in CO_2. *Paleoceanogr. Paleoclimatol.* **38**, e2023PA004666 (2023).
31. Menviel, L. et al. Southern Hemisphere westerlies as a driver of the early deglacial atmospheric CO_2 rise. *Nat. Commun.* **9**, 2503 (2018).
32. Schmitt, J. et al. Carbon isotope constraints on the deglacial CO_2 rise from ice cores. *Science* **336**, 711–714 (2012).
33. Jeltsch-Thömmes, A. & Joos, F. Modeling the evolution of pulse-like perturbations in atmospheric carbon and carbon isotopes: the role of weathering–sedimentation imbalances. *Clim* **16**, 423–451 (2020).
34. Bogotá-A, R. G. et al. Rapid climate change from north Andean Lake Fúquene pollen records driven by obliquity: implications for a basin-wide biostratigraphic zonation for the last 284 ka. *Quat. Sci. Rev.* **30**, 3321–3337 (2011).
35. Zech, W. et al. Obliquity forcing of Quaternary glaciation and environmental changes in NE Siberia. *Quat. Int.* **234**, 133–145 (2011).
36. Li, T. et al. Continued obliquity pacing of East Asian summer precipitation after the mid-Pleistocene transition. *Earth Planet. Sci. Lett.* **457**, 181–190 (2017).
37. Ferreira, J. Q. et al. Changes in obliquity drive tree cover shifts in eastern tropical South America. *Quat. Sci. Rev.* **279**, 107402 (2022).
38. Bosmans, J. H. C., Hilgen, F. J., Tuenter, E. & Lourens, L. J. Obliquity forcing of low-latitude climate. *Clim* **11**, 1335–1346 (2015).
39. Joannin, S., Bassinot, F., Nebout, N. C., Peyron, O. & Beaudouin, C. Vegetation response to obliquity and precession forcing during the Mid-Pleistocene transition in western Mediterranean region (ODP site 976). *Quat. Sci. Rev.* **30**, 280–297 (2011).
40. Claussen, M., Fohlmeister, J., Ganopolski, A. & Brovkin, V. Vegetation dynamics amplifies precessional forcing. *Geophys. Res. Lett.* **33**, L09709 (2006).
41. Caesar, L., Rahmstorf, S., Robinson, A., Feulner, G. & Saba, V. Observed fingerprint of a weakening Atlantic Ocean overturning circulation. *Nature* **556**, 191–196 (2018).

42. Lenton, T. M. et al. Climate tipping points—too risky to bet against. *Nature* **575**, 592–595 (2019).
43. He, F. & Clark, P. U. Freshwater forcing of the atlantic meridional overturning circulation revisited. *Nat. Clim. Chang.* **12**, 449–454 (2022).
44. Bereiter, B. et al. Revision of the EPICA Dome C CO_2 record from 800 to 600 kyr before present: analytical bias in the EDC CO_2 record. *Geophys. Res. Lett.* **42**, 542–549 (2015).
45. Menking, J. A. Multiple carbon cycle mechanisms associated with the glaciation of Marine Isotope Stage 4. *Nat. Commun.* **13**, 5443 (2022).
46. Shin, J. et al. Millennial variations in atmospheric CO_2 during the early Holocene (11.7–7.4 ka). *Clim* **18**, 2063–2075 (2022).
47. Bauska, T. K. et al. Links between atmospheric carbon dioxide, the land carbon reservoir and climate over the past millennium. *Nat. Geosci.* **8**, 383–387 (2015).
48. Loulergue, L. et al. Orbital and millennial-scale features of atmospheric CH_4 over the past 800,000 years. *Nature* **453**, 383–386 (2008).
49. Spahni, R. et al. Atmospheric methane and nitrous oxide of the late pleistocene from Antarctic ice cores. *Science* **310**, 1317–1321 (2005).
50. Jouzel, J. et al. Orbital and millennial antarctic climate variability over the past 800,000 years. *Science* **317**, 793–796 (2007).
51. Buizert, C. et al. The WAIS Divide deep ice core WD2014 chronology–part 1: methane synchronization (68–31 ka BP) and the gas age–ice age difference. *Clim* **11**, 153–173 (2015).
52. Sigl, M. et al. The WAIS Divide deep ice core WD2014 chronology–part 2: Annual-layer counting (0–31 ka BP). *Clim. Past* **12**, 769–786 (2016).

Methods

Atmospheric CO_2 measurements on the EDC ice core

Atmospheric CO_2 measurements on the EDC ice core have been performed at Institut des Geosciences de l'Environnement (IGE) using the ball mill dry-extraction system coupled with a gas chromatograph[12,13]. A total of 203 depth levels have been measured between 2,043.8 and 2,360.6 m corresponding to the time period from 258.6 to 190.0 ka on the AICC2023 gas timescale[22] (Fig. 1). Each data point corresponds to air extracted from a single ice sample of 40 g, and the resulting CO_2 amount fraction is the average of five successive injections of the same air sample made at different pressure levels in the gas chromatograph. The pooled standard deviation of the five injections is 0.9 ppm. Thirty injections of a standard gas (synthetic air from Air Liquide) containing 229.5 ± 0.3 ppm of CO_2 in dry air, which were referenced to two primary standards (241.24 ± 0.015 ppm from National Oceanic and Atmospheric Administration (NOAA), JB03097 and 260.26 ± 0.2 ppm from Commonwealth Scientific and Industrial Research Organisation (CSIRO), CSIRO1677), are used to calibrate the gas chromatograph. First, we correct our data for the crushing process CO_2 contamination that is estimated to be on average of 2.6 ± 0.9 ppm (1σ standard deviation), ranging from 1.0 to 5.4 ppm. This correction is necessary as some CO_2 is released from the CO_2 extraction chamber during the crushing process, which is contaminating our extracted air from the ice sample. Blank tests are conducted by measuring the CO_2 concentration of a standard gas of known amount fraction and crushing artificial gas-free ice. The difference between the measured and expected CO_2 amount fraction is attributed to the crushing process itself. The additional CO_2 amount fraction is then converted into CO_2 levels to normalize the correction to the volume of injected gas. Blank measurements were performed for every ten measured samples for each of the four extraction cells. Following the procedure of ref. 12, the CO_2 data are then corrected for gravitational fractionation occurring in the firn. For that we use a record of the isotopic composition of nitrogen in the trapped air covering our studied time interval ($\delta^{15}N$ of N_2)[53] (not shown here). The average correction is −1.4 ± 0.3 ppm (1σ standard deviation), ranging from −0.9 to −2.1 ppm. The average overall propagated uncertainty of the CO_2 amount fractions is 1.3 ppm. This uncertainty includes the uncertainty related to the five injections (one standard deviation), the uncertainty of the measurement system as determined by standard gas over blank ice measurements (one standard deviation) and the uncertainty associated with and the correction for gravitational settling based on $\delta^{15}N$ corrections.

Over the 260–190-ka time interval, the existing composite CO_2 record[44] includes data measured on the Vostok ice core, associated with a temporal resolution of ~0.85 ka (ref. 13) (Supplementary Fig. 1). The comparison between our new EDC and the Vostok CO_2 records reveals an offset already observed in ref. 12 where these data had been measured using an earlier version of the ball mill extraction system. Especially, the Vostok CO_2 concentrations are slightly higher by 5.5 ppm on average. This offset can be explained by the fact that the Vostok CO_2 measurements were not corrected for the gravitational fractionation and no blank correction was applied[13]. When we apply these two corrections on the Vostok CO_2 record, the observed offset is reduced to ~1.5 ppm (Supplementary Fig. 1).

High-resolution CO_2 data compilation

In addition to this study, four multi-centennial-scale resolved atmospheric CO_2 datasets have been published since the atmospheric CO_2 composite record from ref. 44 was compiled (Fig. 1). Data presented in Fig. 1 are plotted as published and no corrections have been applied. However, this does not affect the results of our study as we focus our analysis on the relative and not absolute variations of CO_2 amount fractions. If we add the duration of all periods with a resolution better than 0.5 ka, we obtain a cumulative duration of 275 ka (vertical red areas, Fig. 1) covering 429 to 329 ka (ref. 1), 258 to 200 ka (this study), 188 to 153 ka (ref. 12) and 84 to 0 ka (refs. 8,45–47,54–56). These periods associated with sub-millennial-scale CO_2 resolution allow us to identify centennial-scale abrupt variability of atmospheric CO_2 (Fig. 2). In the case of ref. 12, results of the CDJ identification should be taken with caution as experimental-induced noise make it hard to distinguish natural centennial-scale variability from measurement-induced noise (Supplementary Fig. 11). Especially, potential CDJs during this time interval could have been missed. The point-to-point variability registered during some periods of the record (186–183 ka; 170–168 ka) confirms that any interpretation of centennial-scale variability during this period needs to carefully take into account this higher variability. We consider that apart from the 429–329 ka, 258–200 ka, 188–153 ka and the 84–0 ka periods (Fig. 2), potential CDJ occurrences are not identifiable due to insufficient temporal resolution and larger uncertainty associated with the Vostok data. In addition, ice older than 500 ka is affected by strong thinning and higher-resolution CO_2 measurements should be performed in the future, in particular taking advantage of new semi-continuous analytical techniques[57].

Atmospheric CH_4 measurements on the EDC ice core

CDJ+ have been linked to atmospheric CH_4 releases of more than 50 ppb (ref. 1) in the ice-core record. However, their identification requires multi-centennial-scale resolution of the CH_4 record. Three of the CDJs identified in this study show a potential CH_4 variability but the associated resolution (>0.5 kyr) was not good enough to validate the occurrence of a synchronous CH_4 increase. The existing CH_4 EDC record for Marine Isotopic Stage (MIS) 8a–6e is based on measurements performed on the IGE and the University of Bern experimental set-ups[48]. We perform 18 measurements on the time interval of the CDJ+7a, CDJ 7b and CDJ−8a.2 to detect a potential CH_4 rise associated with these events. These CH_4 measurements on the EDC ice core were performed at IGE using a melt–refreezing extraction method coupled with a gas chromatograph. The method used for the analysis of these samples is identical to that described in ref. 48. Each sample represents ~40 g of ice from which the air is extracted with a melt–refreezing method. The air is then analysed with a gas chromatograph. Fifteen injections of a single standard gas (synthetic air from Air Liquide) containing 498.1 ± 2.7 ppb of CH_4 in dry air, which was referenced to one primary standard 393.9 ± 2.6 ppb from CSIRO, CSIRO1657), are used to calibrate the gas chromatograph. The average CH_4 analytical uncertainty is 5 ppb (1σ). We do not correct the concentration for gravitational enrichment to avoid an offset with the previously published record from ref. 48. Corrections would be ~3 ppb on average, less than 1% of the CH_4 concentrations signal[48]. A total of 18 depth levels has been measured focusing on the depth interval where centennial-scale atmospheric CO_2 releases have been identified. All samples are corrected for blank contributions using gas-free ice. All CH_4 data are shown in Supplementary Fig. 1.

Identification of the centennial-scale CO_2 events

To identify the presence of CDJs in our CO_2 record between 260 and 190 ka, we follow the method developed by ref. 1. We can summarize this methodology as follows: first, we remove the orbital- and millennial-scale trend in the CO_2 record using smoothing splines[14] with a cut-off frequency ranging from 6 to 14 ka to evaluate the best detrending method. The definition of the cut-off frequency is derived from equation (9) of ref. 14. It corresponds to the period at which 50% of the signal is attenuated by the spline-fitting process. The aim is to find a good compromise between removing multi-millennial- to orbital-scale trends while preserving the centennial-scale variability (Supplementary Fig. 2). Then, a second series of splines ranging from 0.4 to 1.2 ka is applied on the detrended CO_2 record to obtain evenly spaced records aiming at smoothing out measurement uncertainty while still preserving the centennial-scale variability. Third, the rate of change of the final residual CO_2 record is computed (Fig. 3 and Supplementary Fig. 2). To identify a CDJ, we apply the thresholds of

1.5 ppm per century and 5 ppm as in ref. 1. For the 188 to 153 ka (ref. 12) and 84 to 0 ka (refs. 8,45–47,54–56) intervals, we use the exact same method of identification (Supplementary Figs 11–13). For the 429- to 329-ka interval, we compile the CDJs already identified using the same method[1].

Other detection methods of centennial-scale variability have previously been applied during the last glacial period and the last deglaciation. The approach from ref. 17 is based on the analysis of the raw curve of CO_2 concentrations without any corrections to remove the orbital- or the millennial-scale trends. Such an approach is appropriate to identify the centennial-scale atmospheric CO_2 changes of the last termination as the record is very highly resolved (<0.1 ka). In addition, the centennial-scale variability is of such magnitude (~12 ppm) that it prevents any error of identification. Recently, ref. 8 applied a new approach for the identification of the centennial-scale atmospheric CO_2 variability, using the δD record measured on the ice. On the basis of the assumption that this local surface temperature proxy does not include centennial-scale climate variability during the studied intervals[17], they use δD as a filter for identifying centennial-scale CO_2 release. The first step is to estimate the phase relationship between CO_2 and δD to align the two records. Then, by subtracting a normalized δD curve to the CO_2 record, they obtain a residual CO_2 signal. This method is well adapted to identify centennial-scale CO_2 release during the last glacial period, where millennial-scale variability is the dominant climatic pattern. Such an approach assumes that δD is a template for millennial-scale CO_2 variability, which is not the case for all time periods, especially during deglaciations[58–60] and the end of interglacials[61]. The coupling between δD and CO_2 during the 260–190-ka interval, which is mainly composed of a deglaciation and an interglacial period, is thus not trivial. In addition, with that method, all centennial-scale variability of the carbon cycle is investigated. Hence, we consider that the method of ref. 1 based on the smoothing spline is most adapted for the identification of the largest centennial-scale atmospheric CO_2 releases, that is, the CDJ events.

Note that applying the ref. 1 methodology to the most recent period (70–0 ka), where the methodology of ref. 8 was originally used to identify potential CDJs (Supplementary Fig. 13), led to the same results. Also, the coherency between the two methodologies used for the identification of centennial-scale CO_2 release underlines that the main result of the study, that is, the influence of the obliquity on the occurrence of such events, is not dependent on the choice of the CDJ detection method.

Centennial-scale variability in a recent atmospheric CO_2 record measured on the Taylor glacier ice core has been observed during the Marine Isotope Stage 5–4 transition[45]. However, the short time interval covered by the high-resolution CO_2 record (~13 ka) and the absence of water isotope measurements in the same ice core prevent to apply directly the CDJ methodology identification from ref. 1 or from ref. 8. To circumvent this issue, we merged the record from ref. 45 and refs. 56,62 to produce a continuous record over the 90–45-ka interval (Supplementary Fig. 14). We then applied the method of ref. 1 to this merged record. Note that while applied to the whole interval, this test would only allow identification of CDJs on the 74–59-ka interval, where the atmospheric CO_2 concentration resolution is below 500 years (ref. 45) (Fig. 1 and Supplementary Fig. 12).

Chi-square test

We apply a statistical method to investigate the potential role of the Earth's obliquity in the centennial-scale atmospheric CO_2 variability. The Chi-square method allows to test the null hypothesis that a distribution of a parameter (centennial-scale variability occurrences) versus another (obliquity value) is independent. This method assumes a normal distribution of the probability results for the computation of the confidence level. Such approach was applied to determine the impact of external forcing on the climate system in previous studies[63–65]. For that, we separate the centennial-scale events in two categories depending on whether they occur in the context of an obliquity value above or under the average obliquity of the 12 obliquity cycles of last 500 ka (corresponding to the mean obliquity value of the 494.5–9.5-ka period, that is, 23.33°).

For that, we compute:

$$X = \frac{(\text{observed} - \text{expected})^2}{\text{expected}}$$

With observed the number of centennial-scale events occurring below the average obliquity value of the 12 obliquity cycles of the last 500 ka, here 4, and expected the theoretical value expected under the null hypothesis. The theoretical value would be 11 (that is, half of the total number of detected CDJs) if the studied period would contain as many high-obliquity intervals than low-obliquity periods. However, only 44.1% of the studied period is below the average obliquity value taken as reference (23.33°). The theoretical value is thus 9.7. We found:

$$X = 3.4$$

This value is higher than $\alpha_{0.1}$, the risk at 10% to accept the null hypothesis even if it is wrong, which is 2.7 for a degree of freedom of 1. In other words, the value 2.7 is the 90th percentile of the chi-square distribution[66].

We can thus reject the null hypothesis that the distribution of centennial-scale CO_2 events is independent of the obliquity state with a confidence level of 90%. To test the sensitivity of the chosen threshold (here the average obliquity value of the 12 obliquity cycles of the last 500 ka), we performed a chi-square test for the interval of obliquity values (22.7–23.9°) systematically reached during each obliquity cycle over the last 500 ka (Supplementary Fig. 16). Our analysis reinforces the observation of missing CDJ during low-obliquity periods.

We also apply the chi-square test for Earth's precession and eccentricity parameters using the mean values of the last 500 ka (Supplementary Table 2). The null hypothesis of an independence of centennial-scale CO_2 events from precession and eccentricity context could not be rejected at a confidence level of 90%.

Experimental design of carbon cycle modelling

To understand the processes that could lead to a different response of the carbon cycle during an AMOC shutdown as a function of obliquity, numerical experiments are performed with the Earth system model LOVECLIM[26] (Supplementary Table 4). LOVECLIM includes a free surface primitive equation ocean model with a horizontal resolution of 3° × 3° and 20 unevenly spaced vertical levels, a dynamic/thermodynamic sea-ice model, a quasi-geostrophic T21 atmospheric model, a dynamic global vegetation model (DGVM) and a marine carbon cycle model. The DGVM used, VECODE (Vegetation Continuous Description model), simulates the vegetation structure and associated terrestrial carbon reservoirs[26].

The initial 49-ka state was derived from a transient experiment that started at 140 ka. The penultimate deglaciation (140–120 ka) followed the PMIP4 protocol[67], with the model being forced by changes in orbital parameters[68], atmospheric greenhouse gases[69] and changes in continental ice sheets[67]. That simulation was continued between 120 and 49 ka forced with estimates of changes in continental ice sheets from an offline simulation[70]. The Bering Strait was gradually closed at 70 ka and kept closed until the early Holocene.

From that initial state at 49 ka, the model was run for 4,000 years with prognostic atmospheric CO_2 concentration and under constant 49-ka boundary conditions (*HighOblCTR*). The last 1,000 yrs of this experiment serve as control run for the 49-ka experiments (Supplementary Fig. 17).

From the initial transient state, another experiment was run under 49-ka boundary conditions but with an obliquity of 22.1°. This experiment was first run for 4,000 years with a constant atmospheric CO_2 concentration of 204 ppm, after which the CO_2 was prognostic for 2,000 years (*LowOblCTR*) (Supplementary Fig. 17).

From these control runs (*HighOblCTR* and *LowOblCTR*), two meltwater experiments were performed (*HighObl* and *LowObl*) by adding 0.3 Sv of meltwater into the North Atlantic (60–10° W, 50 60° N) for 1,000 years thus leading to an AMOC shutdown in ~300 years. The meltwater flux was then stopped for 800 years, after which a negative meltwater flux was added to the North Atlantic (−0.1 Sv) for 400 years so that the AMOC would recover.

Two experiments with similar forcing to HighObl and LowObl but with a 40% increase of the westerly wind stress over the Southern Ocean between 65° S and 34° S from year 0 to 1,800 (*HighObl_SHW* and *LowObl_SHW*) were also performed.

Finally, two experiments similar to *HighObl* and *LowObl* and two experiments similar to *HighObl_SHW* and *LowObl_SHW* were performed in which the terrestrial carbon fluxes did not impact atmospheric CO_2 (*HighObl_NoVeg*, *LowObl_NoVeg*, *HighObl_NoVeg_SHW* and *LowObl_NoVeg_SHW*). Note that for these experiments, the model was first run for 2,000 years without any meltwater so that the atmospheric CO_2 concentration would equilibrate.

We also perform some numerical experiments to better understand the carbon cycle response to CDJ+. This is, however, challenging as the climatic conditions associated with CDJ+ are poorly known, implying that the background climatic conditions and AMOC change associated with these events are poorly constrained. Nevertheless, one CDJ+ is identified at the end of the Younger Dryas, when the obliquity is high (24.16°). Starting from a transient simulation of the last deglaciation[31], we branch an equilibrium simulation forced with constant boundary conditions (that is, orbital parameters, ice-sheet configuration and albedo, Bering Strait open) representing 12 ka but with interactive atmospheric CO_2 (*YDctr*). A similar equilibrium experiment is performed but with low obliquity (22.1°, *YD-lowOblctr*). From these equilibrium states, 0.16 Sv of freshwater is added into the North Atlantic for 1,000 years to simulate an AMOC weakening (*YDNA* and *YDlowOblNA*) (Supplementary Fig. 21).

Data availability

The atmospheric CO_2 and CH_4 data are available at https://doi.pangaea.de/10.1594/PANGAEA.972146 (ref. 69) and https://doi.pangaea.de/10.1594/PANGAEA.972147 (ref. 70). The output simulations are available at http://hdl.handle.net/1959.4/102810 (https://doi.org/10.26190/unsworks/30408) (ref. 71).

Code availability

The simulations are based on the LOVECLIM model version 1.2, with code accessible at http://www.elic.ucl.ac.be/modx/elic/index.php?id=289.

References

53. Ahn, J. & Brook, E. J. Siple Dome ice reveals two modes of millennial CO_2 change during the last ice age. *Nat. Commun.* **5**, 3723 (2014).
54. Bereiter, B. et al. Mode change of millennial CO_2 variability during the last glacial cycle associated with a bipolar marine carbon seesaw. *Proc. Natl Acad. Sci. USA* **109**, 9755–9760 (2012).
55. Mächler, L. et al. Laser-induced sublimation extraction for centimeter-resolution multi-species greenhouse gas analysis on ice cores. *Atmos. Meas. Tech.* **16**, 355–372 (2023).
56. Parrenin, F. et al. Synchronous change of atmospheric CO_2 and antarctic temperature during the last deglacial warming. *Science* **339**, 1060–1063 (2013).
57. Chowdhry Beeman, J. et al. Antarctic temperature and CO_2: near-synchrony yet variable phasing during the last deglaciation. *Clim* **15**, 913–926 (2019).
58. Landais, A. et al. Two-phase change in CO_2, Antarctic temperature and global climate during Termination II. *Nat. Geosci.* **6**, 1062–1065 (2013).
59. Ai, X. E. et al. Southern Ocean upwelling, Earth's obliquity, and glacial–interglacial atmospheric CO_2 change. *Science* **370**, 1348–1352 (2020).
60. Lüthi, D. et al. CO_2 and O_2/N_2 variations in and just below the bubble–clathrate transformation zone of Antarctic ice cores. *Earth Planet. Sci. Lett.* **297**, 226–233 (2010).
61. Liautaud, P. R., Hodell, D. A. & Huybers, P. Detection of significant climatic precession variability in early Pleistocene glacial cycles. *Earth Planet. Sci. Lett.* **536**, 116–137 (2020).
62. Huybers, P. & Wunsch, C. Obliquity pacing of the late Pleistocene glacial terminations. *Nature* **434**, 491–494 (2005).
63. Lohmann, J. & Svensson, A. Ice core evidence for major volcanic eruptions at the onset of Dansgaard–Oeschger warming events. *Clim* **18**, 2021–2043 (2022).
64. Efron, B. & Morris, C. Data analysis using Stein's estimator and its generalizations. *J. Am. Stat. Assoc.* **70**, 311–319 (1975).
65. Menviel, L. et al. The penultimate deglaciation: protocol for Paleoclimate Modelling Intercomparison Project (PMIP) phase 4 transient numerical simulations between 140 and 127 ka, version 1.0. *Geosci. Model Dev.* **12**, 3649–3685 (2019).
66. Berger, A. L. Long-term variations of caloric insolation resulting from the earth's orbital elements. *Quat. Res.* **9**, 139–167 (1978).
67. Köhler, P., Nehrbass-Ahles, C., Schmitt, J., Stocker, T. F. & Fischer, H. A 156 kyr smoothed history of the atmospheric greenhouse gases CO_2, CH_4, and N_2O and their radiative forcing. *Earth Syst. Sci. Data* **9**, 363–387 (2017).
68. Abe-Ouchi, A. et al. Insolation-driven 100,000-year glacial cycles and hysteresis of ice-sheet volume. *Nature* **500**, 190–193 (2013).
69. Legrain, E. et al. High-resolution atmospheric CO_2 records derived from the EPICA Dome C ice core covering 260-190ka (MIS 8a - 7a). *PANGAEA* https://doi.org/10.1594/PANGAEA.972146 (2024).
70. Legrain, E. et al. High-resolution atmospheric CH_4 records derived from the EPICA Dome C ice core covering 260-190ka (MIS 8a - 7a). *PANGAEA* https://doi.org/10.1594/PANGAEA.972147 (2024).
71. Menviel, L. et al. Atmospheric CO_2 response to AMOC changes under high and low obliquity. *UNSW Library* https://doi.org/10.26190/unsworks/30408 (2024).

Acknowledgements

This study is an outcome of the Make Our Planet Great Again HOTCLIM project; it received the financial support from the French National Research Agency under the 'Programme d'Investissements d'Avenir' (ANR-19-MPGA-0001). This publication was also generated in the frame of the Beyond EPICA Oldest Ice Core (BE-OI) project. The BE-OI project has received funding from the European Union's Horizon 2020 research and innovation programme under grant agreement number 815384 (Oldest Ice Core). It is supported by national partners and funding agencies in Belgium, Denmark, France, Germany, Italy, Norway, Sweden (through the Crafoord Foundation) and Switzerland, the Netherlands and the United Kingdom. Logistic support is mainly provided by Agenzia Nazionale per le nuove tecnologie, l'nergia e lo sviluppo economico sostenibile (ENEA) and Institut polaire français Paul-Emile Victor (IPEV) through the Concordia Station system. The opinions expressed and arguments employed herein do not necessarily reflect the official views of the European Union funding agency or other national funding bodies. This is Beyond EPICA publication number 39. E.L. was also supported by the Belgian Federal Science Policy Office (BELSPO; FROID project).

E.C. also acknowledges financial support from the AXA Research Fund. L.M. acknowledges funding from the Australian Research Council (ARC) grants FT180100606 and SR200100008. The research leading to these results has received funding from the French National Research Agency (ANR HUMI17 and ANR NEANDROOT) and the European Research Council under the European Union Horizon 2020 Programme (ERC ICORDA, grant number 817493). T.F.S. and H.F. gratefully acknowledge funding by the Swiss National Science Foundation (grants 200020_200492 and 200020_200328, respectively). The LOVECLIM experiments were performed on the computational cluster Katana supported by Research Technology Services at UNSW Sydney. We thank NOAA's Pacific Marine Environmental Laboratory for the use of Ferret.

Author contributions

E.L., E.C. and L.M. designed research. E.L., G.T. and A.W. performed the experimental analyses. L.M. performed the modelling work. E.L. and E.C. wrote a draft with subsequent inputs from all co-authors.

Competing interests

The authors declare no competing interests.

Additional information

Supplementary information The online version contains supplementary material available at https://doi.org/10.1038/s41561-024-01556-5.

Correspondence and requests for materials should be addressed to Etienne Legrain.

Peer review information *Nature Geoscience* thanks the anonymous reviewers for their contribution to the peer review of this work. Primary Handling Editor: Alison Hunt, in collaboration with the *Nature Geoscience* team.